


# DFT computational insights into structural, electronic and spectroscopic parameters of 2-(2-Hydrazineyl)thiazole derivatives: a concise theoretical and experimental approach

Vishnu A. Adole , Thansing B. Pawar & Bapu S. Jagdale

To cite this article: Vishnu A. Adole , Thansing B. Pawar & Bapu S. Jagdale (2020): DFT computational insights into structural, electronic and spectroscopic parameters of 2-(2-Hydrazineyl)thiazole derivatives: a concise theoretical and experimental approach, Journal of Sulfur Chemistry, DOI: [10.1080/17415993.2020.1817456](https://doi.org/10.1080/17415993.2020.1817456)

To link to this article: <https://doi.org/10.1080/17415993.2020.1817456>

 View supplementary material 

 Published online: 14 Sep 2020.

 Submit your article to this journal 


 Article views: 10

 View related articles 

 View Crossmark data 



# DFT computational insights into structural, electronic and spectroscopic parameters of 2-(2-Hydrazineyl)thiazole derivatives: a concise theoretical and experimental approach

Vishnu A. Adole <sup>a</sup>, Thansing B. Pawar<sup>b</sup> and Bapu S. Jagdale<sup>a</sup>

<sup>a</sup>Department of Chemistry, Arts, Science and Commerce College, Manmad, Nashik, India; <sup>b</sup>Department of Chemistry, Loknete Vyankatrao Hiray Arts, Science and Commerce College Panchavati, Nashik, India

## ABSTRACT

It has been uncovered that compounds containing thiazole moiety display noteworthy biological properties, which have attracted the attention of many researchers in chemical biology as well as in medicinal chemistry. In the current examination, ten 2-(2-hydrazineyl)thiazole derivatives were studied using density functional theory (DFT). The geometry of all ten molecules was optimized by employing the DFT method with the B3LYP/6-311G (d,p) basis set. For the detailed structural and spectroscopic examination, the (*E*)-4-phenyl-2-(2-(1,2,6,7-tetrahydro-8*H*-indeno[5,4-*b*]furan-8-ylidene)hydrazineyl)thiazole (**PIFHT**) was studied as a representative molecule. The bond lengths and bond angles of the **PIFHT** molecule were discussed for the detailed understanding of the structural entities. The electronic parameters of all ten molecules were analyzed by computing HOMO and LUMO pictures. Using frontier molecular orbital analysis, spectroscopic and quantum chemical parameters were evaluated and discussed to explore the chemical reactivity of the molecules. Besides, absorption energies, oscillator strength, and electronic transitions of **PIFHT** molecule were explored using time-dependent density-functional theory (TD-DFT) at the B3LYP/6-311G (d,p) level of theory in the gas phase, dichloromethane, and dimethyl sulfoxide solvents. The TD-DFT computed theoretical UV-Visible spectra of the **PIFHT** molecule were compared with the experimental UV-Visible spectra. The scaled vibrational frequencies were compared with the experimental frequencies for the assignment of the vibrational bands. The comparisons between computed and experimental UV-Visible and IR spectral results are gratifying. The molecular electrostatic surface potential plots were computed for locating the reactivity sites. Mulliken atomic charges were also studied for acquiring insights into charge density.


## ARTICLE HISTORY

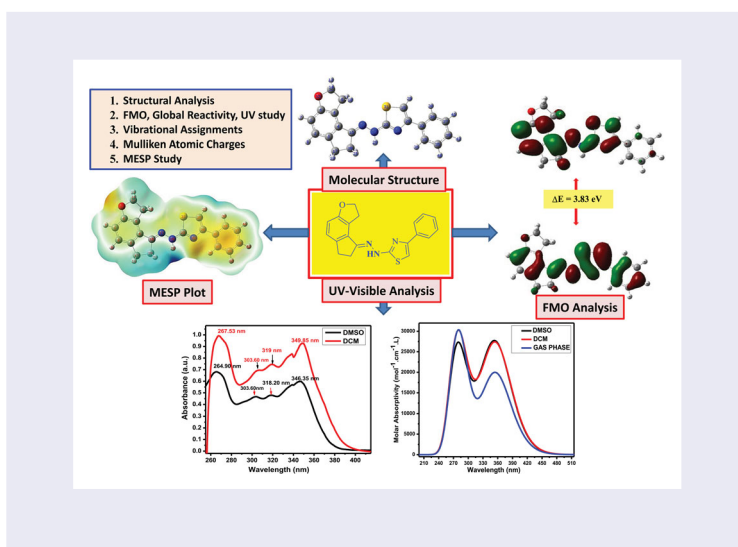
Received 24 March 2020  
Accepted 23 August 2020

## KEYWORDS

Density functional theory; B3LYP/6-311G (d,p); 2-(2-Hydrazineyl)thiazole derivatives; frontier molecular orbital; molecular electrostatic surface potential

**CONTACT** Vishnu A. Adole  vishnuadole86@gmail.com  Department of Chemistry, Arts, Science and Commerce College, Manmad, Nashik-423 104, MH, India

 Supplemental data for this article can be accessed here. <https://doi.org/10.1080/17415993.2020.1817456>



## 1. Introduction

The thiazole structure is a vital pharmacophore in the domain of science; in light of its omnipresence in a variety of biological properties [1–5]. The hydrazinylthiazolyl core is one of the significant pharmacological scaffolds which have produced a profound interest in medicinal and industrial researchers. The astounding pharmacological profile of hydrazinylthiazolyl derivatives includes antitubercular, antimalarial, anti-inflammatory, antitumor, antiproliferative, antioxidant, and antimicrobial activity [6–13]. Besides, numerous thiazole hybrids have been identified as potential antibacterial [14–16], anticancer [17,18], anti-inflammatory [19], anti-tubercular [20], antioxidant [21], analgesic [21,22], antidiabetic [23,24], anti-Alzheimer agents [25,26]. The remarkable examples which show diverse biological activities are depicted in Figure 1. For instance, ravuconazole inhibits 14 $\alpha$  demethylase prompting lysis of the fungal cell wall and responsible for fungal cell death [27,28]. Niridazole is used to cure schistosomiasis (helminthic disease) caused by some flatworms of the genus *Schistosoma* [29]. Thiamine injections are used to prevent or cure vitamin B1 deficiency [30,31]. Thiabendazole drug is being used for the treatment of infections caused by worms, for example, threadworm [32,33]. Aztreonam is an antibiotic and principally used to treat diseases brought about by gram-negative bacteria, for example, *Pseudomonas aeruginosa* [34,35]. Ravuconazole is used to treat fungal infections and therefore act as an antimicrobial agent [36,37]. Voreloxin has a double anti-cancer activity that combines DNA intercalation and the suppression of topoisomerase II action [38,39]. Appropriately, it seems, by all accounts, to be exceedingly appealing to study the previously synthesized 2-(2-hydrazinyl) thiazole derivatives [40] of biological intrigue from a computational investigation point of view.

DFT-based computational studies play a vital role in identifying the new drug candidates. The quantum chemical data obtained from DFT has been effectively used in

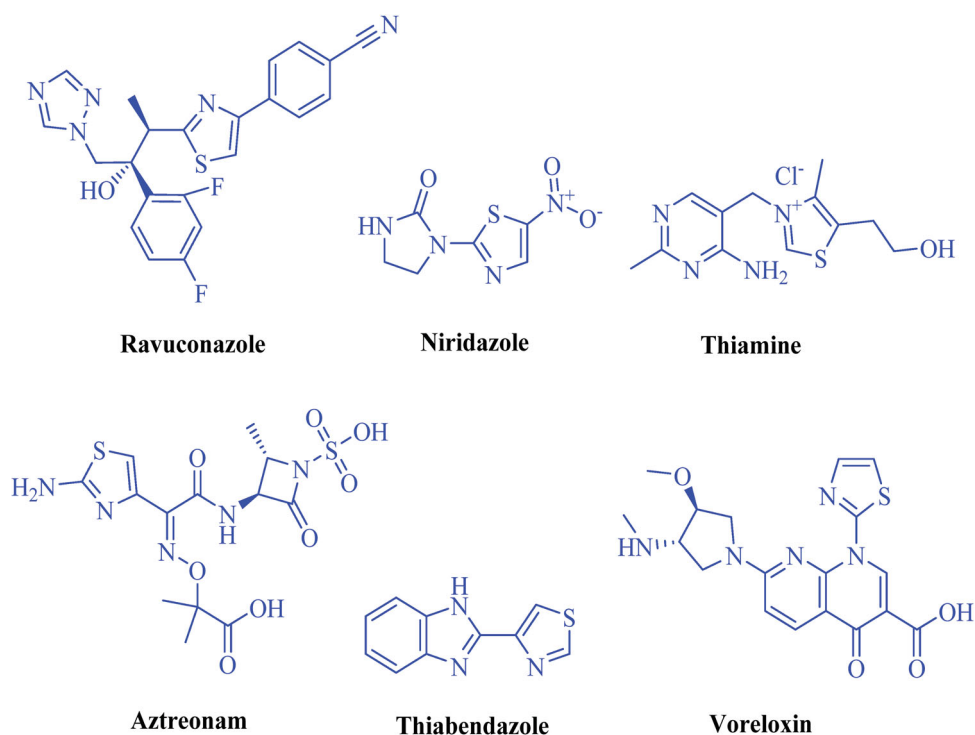


**Figure 1.** Some thiazole containing commercial drugs.

various fields [41–46]. Due to computational chemistry, it has become feasible to foresee many physical and chemical properties of the molecules. A literature survey reveals that theoretical calculations and empirical experiments are expected to affirm one another [47–50]. All the more definitely, UV-Visible and FT-IR spectral assignments have become effortless with the help of theoretical computations [51–56]. The usefulness of spectroscopic and quantum calculations have been proved to be essential to envisage various spectroscopic aspects of the molecules [57–61]. Crucially, DFT computations have also been used to explore the linear and nonlinear optical properties of the thiazole derivatives [62]. The B3LYP functional and 6-311G (d,p) basis set envisions the optical, spectral, and charge density properties of the molecules more precisely [63–67]. On this premise, we have employed B3LYP with the 6-311G (d,p) basis set for exploring various structural, spectral, and reactivity parameters of the studied compounds. Considering all the indispensable angles mentioned above, the ten 2-(2-hydrazineyl)thiazole derivatives were examined using combined DFT and experimental approach. The molecular properties like optimized molecular structure, bond length, bond angle, Mulliken atomic charges, MESP plots, total energy, HOMO–LUMO energies, charge distribution, ionization potential (I), electron affinity (A), electronegativity ( $\chi$ ), global softness ( $\sigma$ ), absolute hardness ( $\eta$ ), global electrophilicity index ( $\omega$ ), charge transfer ( $\Delta N_{\max}$ ), chemical potential (Pi), etc. have been studied in the present examination. Importantly, theoretical UV-Visible and IR bands were correlated with the experimental UV-Visible and FT-IR bands.

## 2. Results and discussion

### 2.1. Molecular structure and structural analysis

In the present study, ten 2-(2-hydrazinyl)thiazoles (Table 1) have been studied using DFT method with a B3LYP/6-311G (d,p) basis set to determine various structural and chemical parameters. The different abbreviations have been assigned for the 2-(2-hydrazinyl)thiazole derivatives for facile discussion. All ten 2-(2-hydrazinyl)thiazole derivatives are having C1 point group symmetry as predicted by the DFT investigation. The optimized molecular structures are represented in Figure 2. The molecule **NIFHT-2** has the highest polarity ( $\mu = 7.64$  Debye) whereas the molecule **IFHPT** has the lowest polarity ( $\mu = 1.40$  Debye) amongst 2-(2-hydrazinyl)thiazoles (Table S3, supporting information). This can be clarified by considering Figure 3. In the case of **NIFHT-2**, the two groups possessing inverse electronic effects are present at the two termini which prompt the augmentation in the polarity of the molecule. On the other hand, in the case of **IFHPT**, the two terminal groups are having an electron releasing effect, thus, results in a decrease of polarity. The phenomenon of the polarity is extremely crucial to foresee which compounds would enter through the lipophilic membrane of the microorganisms .

The structural parameters like bond lengths and bond angles for the **PIFHT** molecule have been computed by DFT/B3LYP method with the 6-311G (d,p) basis set. The bond length and bond angle data are presented in Table S1 (supporting information). Amongst benzene carbon-carbon double bond lengths, C3-C4 has the highest (1.4071 Å) and C34-C37 has the lowest (1.3896 Å) bond length. The C3-C4 bond length is higher due to the conjugation effect of the alkoxy group from the opposite side. The bond length of an imine bond (C23-N30) of the thiazole ring is 1.2964 Å, whereas the exocyclic imine bond (C16-N27) has 1.2866 Å bond lengths. The former imine bond has a higher value due to the presence of a strong +R effect of the sulfur atom within the thiazole ring. The C23-N28 bond has acquired a partial double bond character due to the resonance effect and has a bond length of 1.3691 Å. The N27-N28 bond length is 1.3545 Å. The C-S bond lengths for the C23-S31 and C25-S31 are 1.7577 and 1.7456 Å, respectively. The C6-O15 and C12-O15 bond lengths are 1.3627 and 1.456 Å, respectively. Amongst C-H bonds, the C20-H21 bond has the longest bond (1.096 Å) and the C33-H36 bond has the shortest bond (1.082 Å). The N28-H29 bond length is 1.0138 Å. The N-H bond is shorter as compared to the C-H bonds due to the strong electronegative effect of a nitrogen atom. The C17-C20 is the longest bond amongst all carbon-carbon bonds with a bond length value of 1.5532 Å. The other computed bond lengths and bond angles are also in good agreement with the structure of **PIFHT** molecule.

### 2.2. Frontier molecular orbital, global descriptors' and UV-visible absorption study

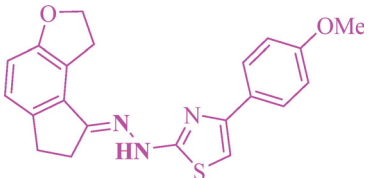
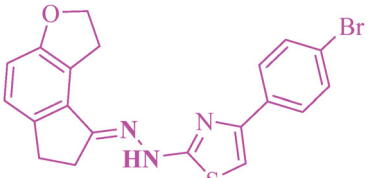
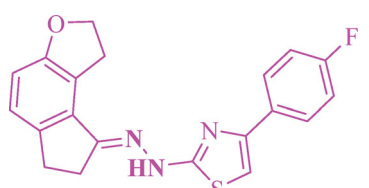
The frontier molecular orbitals (FMO) of the **PIFHT**, **NIFHT-3**, and **CIFHT-2** molecules are presented in Figure 4. The highest occupied molecular orbital (HOMO) and lowest unoccupied molecular orbital (LUMO) are FMO. The FMO pictures of the other seven thiazole derivatives are given in Figure S2 (supporting information). The electronic parameters and global reactivity descriptors' statistics of all ten molecules are given in Table S2 (supporting information) and Table S3 (supporting information), respectively. The global descriptors' statistics were calculated using Koopmans' theorem [68]. The FMO study

**Table 1.** The structures of 2-hydrazinyl thiazole derivatives, systematic names and abbreviation used.

Entry	2-(2-hydrazinyl)thiazoles	Systematic name	Abbreviation used
1		( <i>E</i> )-4-phenyl-2-(2-(1,2,6,7-tetrahydro-8 <i>H</i> -indeno[5,4- <i>b</i> ]furan-8-ylidene)hydrazineyl)thiazole	<b>PIFHT</b>
2		( <i>E</i> )-4-(naphthalen-1-yl)-2-(2-(1,2,6,7-tetrahydro-8 <i>H</i> -indeno[5,4- <i>b</i> ]furan-8-ylidene)hydrazineyl)thiazole	<b>NIFHT-1</b>
3		( <i>E</i> )-2-(2-(1,2,6,7-tetrahydro-8 <i>H</i> -indeno[5,4- <i>b</i> ]furan-8-ylidene)hydrazineyl)-4-( <i>p</i> -tolyl)thiazole	<b>IFHPT</b>
4		( <i>E</i> )-4-(4-nitrophenyl)-2-(2-(1,2,6,7-tetrahydro-8 <i>H</i> -indeno[5,4- <i>b</i> ]furan-8-ylidene)hydrazineyl)thiazole	<b>NIFHT-2</b>
5		( <i>E</i> )-4-(3-nitrophenyl)-2-(2-(1,2,6,7-tetrahydro-8 <i>H</i> -indeno[5,4- <i>b</i> ]furan-8-ylidene)hydrazineyl)thiazole	<b>NIFHT-3</b>
6		( <i>E</i> )-4-(4-chlorophenyl)-2-(2-(1,2,6,7-tetrahydro-8 <i>H</i> -indeno[5,4- <i>b</i> ]furan-8-ylidene)hydrazineyl)thiazole	<b>CIFHT-1</b>
7		( <i>E</i> )-4-(3-chlorophenyl)-2-(2-(1,2,6,7-tetrahydro-8 <i>H</i> -indeno[5,4- <i>b</i> ]furan-8-ylidene)hydrazineyl)thiazole	<b>CIFHT-2</b>

(continued).

**Table 1.** Continued.

Entry	2-(2-hydrazinyl)thiazoles	Systematic name	Abbreviation used
8		(E)-4-(4-methoxyphenyl)-2-(2-(1,2,6,7-tetrahydro-8 <i>H</i> -indeno[5,4- <i>b</i> ]furan-8-ylidene)hydrazineyl)thiazole	<b>MIFHT</b>
9		(E)-4-(4-bromophenyl)-2-(2-(1,2,6,7-tetrahydro-8 <i>H</i> -indeno[5,4- <i>b</i> ]furan-8-ylidene)hydrazineyl)thiazole	<b>BIFHT</b>
10		(E)-4-(4-fluorophenyl)-2-(2-(1,2,6,7-tetrahydro-8 <i>H</i> -indeno[5,4- <i>b</i> ]furan-8-ylidene)hydrazineyl)thiazole	<b>FIFHT</b>

indicates that the **NIFHT-3** has the lowest HOMO–LUMO energy gap ( $E_g = 3.2103$  eV) and the **CIFHT-2** molecule has the highest HOMO–LUMO energy gap ( $E_g = 3.8751$  eV). The reason for this contrasting behavior is the presence of methoxy substituent in the **CIFHT-2** molecule which raises the energy of the HOMO and LUMO and thus increases the energy gap. The lower HOMO–LUMO energy gap in the molecule **NIFHT-3** demonstrates the inevitable charge transfer is eventuating within the molecule, and it is happening smoother as compared to the other thiazole derivatives. Amongst thiazole derivatives, **MIFHT** has more reactive HOMO ( $E_{HOMO} = -5.2000$  eV) and the **NIFHT-2** has less reactive HOMO ( $E_{HOMO} = -5.7372$  eV). The **NIFHT-2** contains powerful electron-withdrawing nitro substituent whereas **MIFHT** has powerful electron releasing methoxy substituent affecting the HOMO energy exactly in the contrast way. The LUMO with more reactivity is present in the **NIFHT-2** ( $E_{LUMO} = -2.5189$  eV) and with less reactivity in the **MIFHT** ( $E_{LUMO} = -1.4939$  eV). The cause is again the presence of substituents with the opposite electronic effect. The molecule with the highest ionization potential is **NIFHT-2** ( $I = 5.7372$  eV) and with the lowest value is **MIFHT** ( $I = 5.2000$  eV). The electron affinity value is higher for the molecule **NIFHT-2** ( $A = 2.7673$  eV) and is lower for the **MIFHT** ( $A = 1.4939$  eV). In brief, the two molecules **NIFHT-2** and **MIFHT** are having exactly opposite electronic and chemical behavior. The concept of hard and soft nature of the molecules is considered an important tool for the assessment of chemical reactivity according to the HSAB principle. As far as global softness is concerned, the **NIFHT-3** is the softest molecule among all thiazole derivatives with a global softness value of  $0.6230$  eV<sup>-1</sup>. The absolute hardness is higher for the **CIFHT-2** molecule ( $\eta = 1.9375$  eV). The ease of removal of an electron is governed by its chemical potential  $P_i$  (eV), and it is likewise identified with its electronegativity. The global descriptor study suggests all these are good



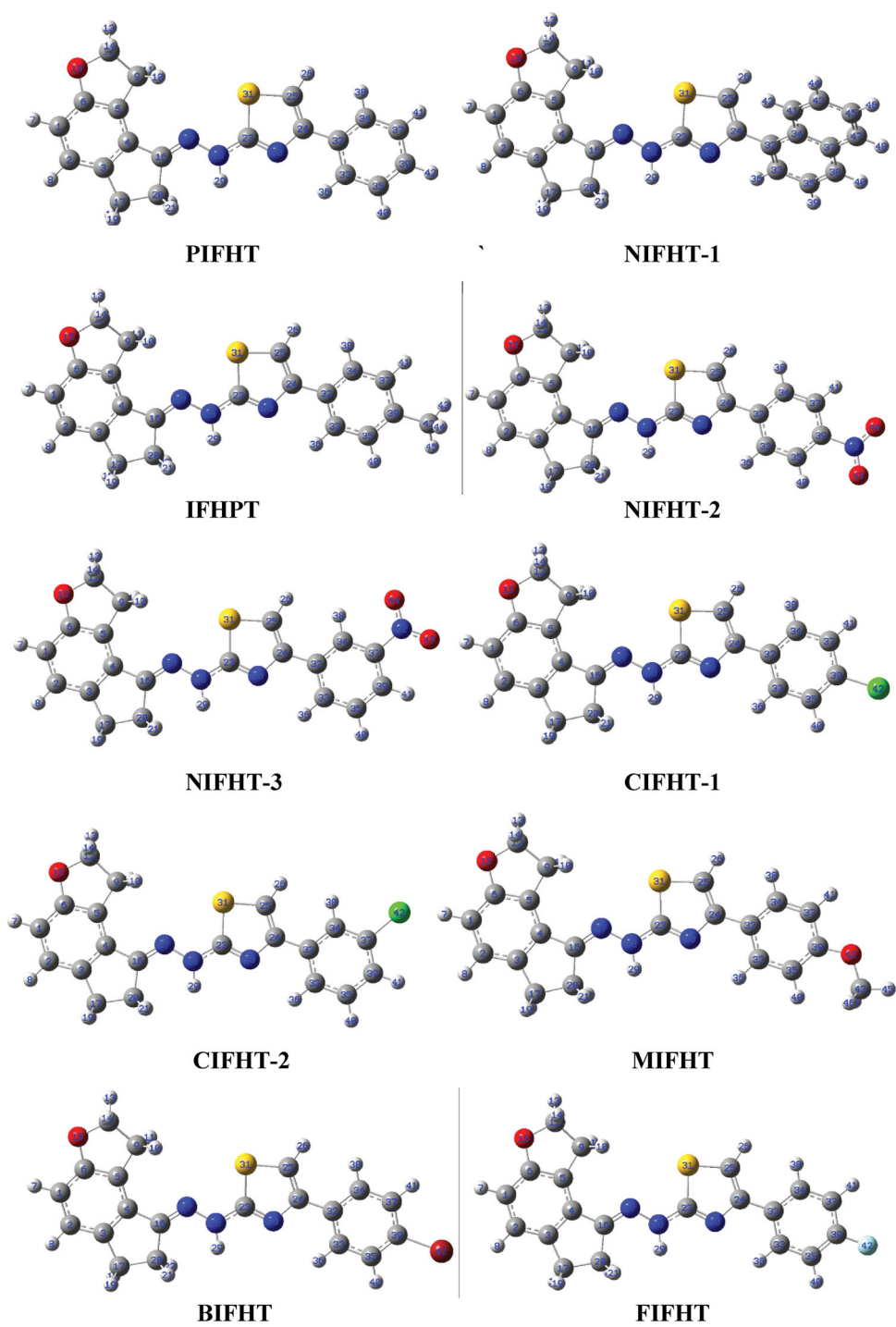


**Figure 2.** Optimized molecular structures of 2-hydrazinyl thiazole derivatives.



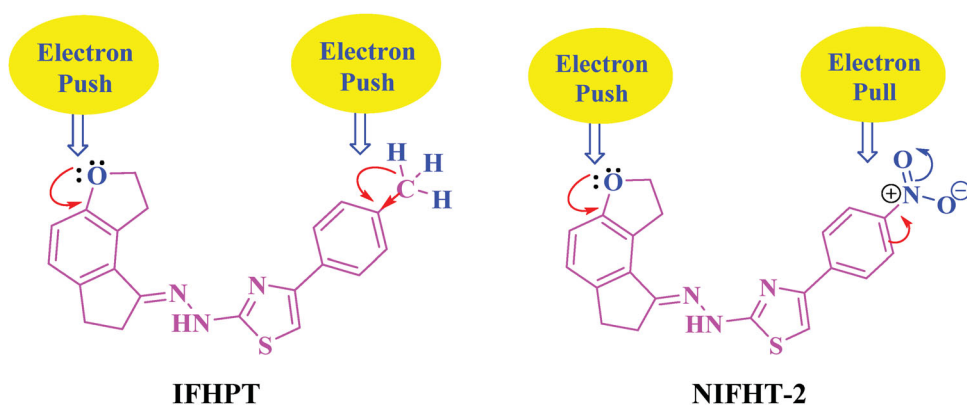


**Figure 3.** The direction of electron movement.

electrophiles as the value of global electrophilicity is more than 1.5 eV. A good electrophile is described by a higher value of the global electrophilicity index and its lower value indicates good nucleophile. Our results suggest that the **NIFHT-2** molecule has a higher value of global electrophilicity index ( $\omega = 5.2948$  eV), so it is most likely to accept electrons readily and would also undergo nucleophilic attack easily. On the other hand, the molecule **MIFHT** has a lower value of global electrophilicity ( $\omega = 3.0225$  eV) indicating that it is a potent nucleophile. As chemical potential ( $P_i$ ) increases, the ability of a molecule to lose an electron increases. The maximum charge transfer is shown by **NIFHT-2** and **NIFHT-3** with charge transfer value of 2.7979 eV. The intramolecular charge transfer (ICT) process in donor-acceptor frameworks has vital significance in various different and biological systems. The ICT and  $\pi \rightarrow \pi^*$  transitions in the titled compounds were established using UV-Visible spectroscopy and theoretical computations. The ICT phenomenon is dominant in the **NIFHT-2** and **NIFHT-3** molecules due to the presence of donor (alkoxy) and acceptor (nitro) substituents at the two end parts of the molecules. These two molecules have also exhibited maximum charge transfer values (Table S3, supporting information).

Absorption energies ( $\lambda$  in nm), oscillator strength ( $f$ ), and electronic transitions of all ten molecules have been computed at the TD-DFT B3LYP/6-311G (d,p) level of theory for B3LYP/6-311G (d,p) optimized geometries. The theoretical absorption energies ( $\lambda$  in nm), oscillator strength ( $f$ ), and transitions of **PIFHT** molecule along with the experimental UV-Visible data have been presented in Table S4 (supporting information). The electronic absorption data of the molecules are given in Table S5 (supporting information). The theoretical UV-Visible absorption data for the **PIFHT** molecule is processed up to four excited states and for the remaining molecules up to one excited state (corresponding to HOMO-LUMO electronic transition only). The experimental UV-Visible spectrum for the **PIFHT** molecule is recorded in the dichloromethane (DCM) and dimethyl sulfoxide (DMSO) solvents and the theoretical UV-Visible spectrum in the gas phase, DCM, and the DMSO solvent. The theoretical UV-Visible spectrum of **PIFHT** is depicted in Figure 5 whereas the experimental UV-Visible spectrum is displayed in Figure 6. The first  $(\pi-\pi^*)^1$  state is centered at 356.43 nm in the gas phase, 357.36 nm in DCM, and 356.77 nm in DMSO as predicted by the theoretical computations. A similar experimental absorption band is located at 349.85 and 346.35 nm in DCM, and DMSO respectively. This outcome

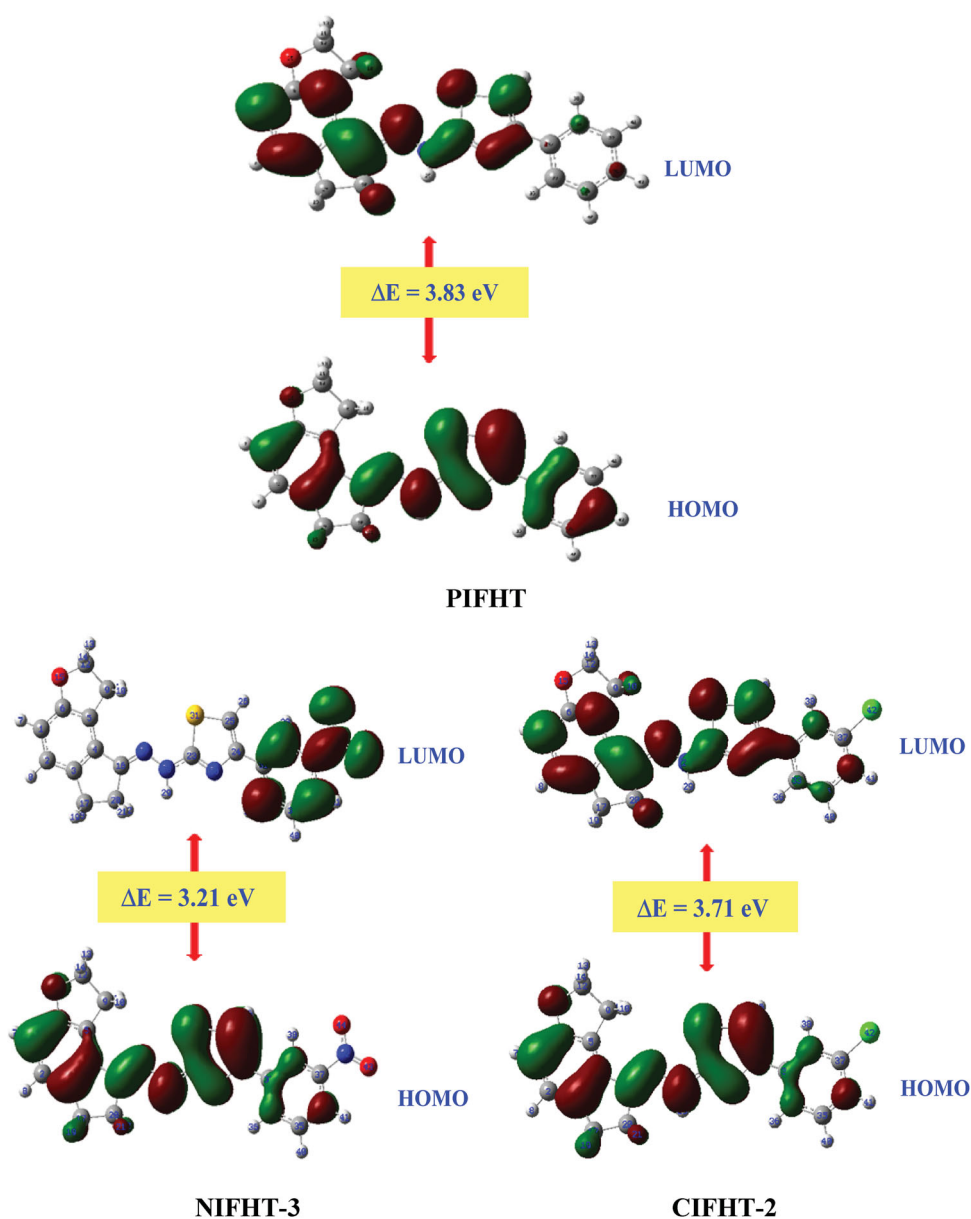


**Figure 4.** Frontier molecular orbital pictures.

implies that theoretical results are in good agreement with the experimental results. The HOMO–LUMO electronic transition corresponds to the 91  $\rightarrow$  92 configurations. The solvents' effect on the HOMO–LUMO absorption wavelength of the **PIFHT** molecule is found to be a bathochromic shift as per theoretical data. The slight augmentation in the absorption wavelength is more in DCM as compared to the DMSO. The second excited state is observed at 321.57 nm (gas phase), 322.00 nm (DCM), and at 321.79 nm (DMSO) in the theoretical spectrum. The same absorption band is located at 319 nm (DCM) and

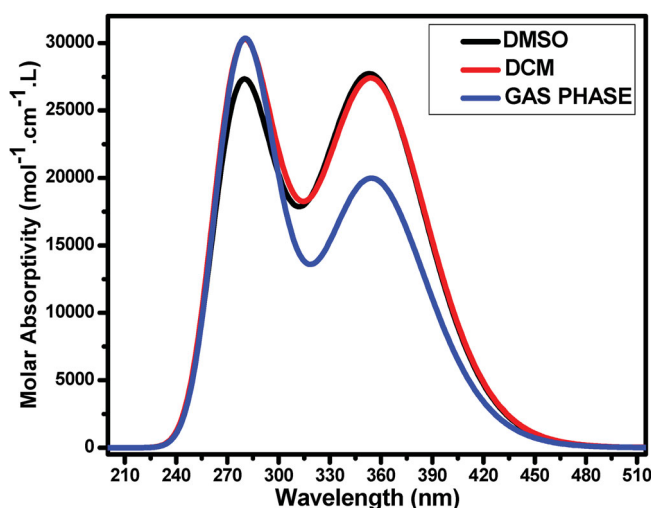


**Figure 5.** Theoretical UV-Visible spectrum of PIFHT in gas phase, DCM, and DMSO.

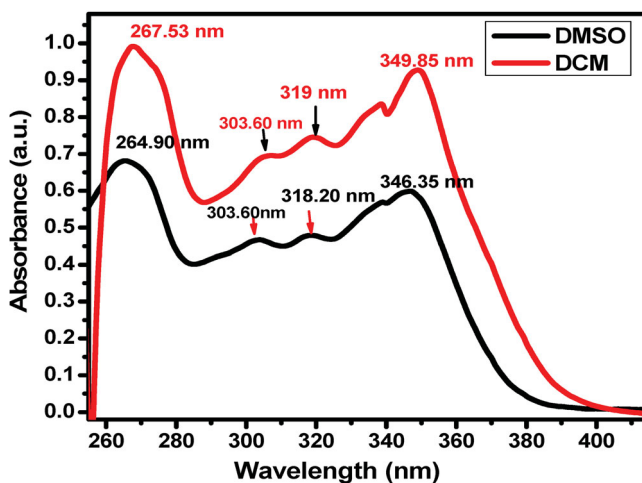


**Figure 6.** Experimental UV-Visible spectrum of PIFHT in DCM and DMSO solvents.

318.20 nm (DMSO) in the experimental analysis. The second singlet excited state relates to the  $90 \rightarrow 92$  configurations. The third singlet excited state band is coming from the two configurations namely  $89 \rightarrow 92$  and  $91 \rightarrow 93$ . This absorption band has values as 302.66 nm (gas phase), 311.82 nm (DCM), and 312.78 nm (DMSO) which are correlated with the experimental value of 303.60 nm (both in DCM and DMSO). The fourth singlet excited state computed theoretically appears at 279.51 nm (gas phase), 278.41 nm (DCM), and 277.95 nm (DMSO). This state is composed of a two (in gas phase), five (in DCM), and four (in DMSO) configurations. This is assigned as a delocalized absorption band having more polarity. Therefore, a greater solvent effect is observed in the experimental analysis. The experimental signals for the fourth excited state are 267.53 nm (DCM) and 264.90 nm (DMSO).

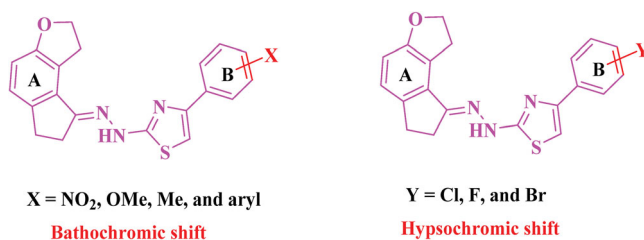


**Figure 7.** Pictorial presentation of the effect of substituents on absorption energies.

The first excited absorption energies ( $\lambda$  in nm), oscillator strength ( $f$ ), and transitions are given in Table S5 (supporting information). In the present exploration, the effect of substituents (attached to ring B) (Figure 7) on absorption energies is also discussed. Our study revealed that the presence of substituents like NO<sub>2</sub>, OMe, Me, and Ar on ring B augmented the absorption wavelength, *i.e.* results in the bathochromic shift. On the contrary, the substituents like Cl, F, and Br have declined the absorption wavelength, *i.e.* results in the hypsochromic shift. The nitro substituent has been linked with a greater increment in the absorption wavelength as compared to the other substituents. This is because of the extended conjugation from the alkoxy substituent up to nitro substituent through aromatic double bonds.

### 2.3. Mulliken atomic charges and molecular electrostatic potential study

The Mulliken atomic charges of the **PIFHT** molecule are calculated by DFT/B3LYP method with 6-311G (d,p) basis set in the gaseous phase are given in Table S6 (supporting information) and also indicated by colors and values in Figure 8. The Mulliken atomic charges revealed that all the hydrogen atoms have a net positive charge. The H29 atom has a more positive charge (0.221481) than other hydrogen atoms and therefore most acidic. The high positive character is due to the attachment with a nitrogen atom. The C6 atom has the highest net positive charge (0.225302) due to the attachment with the electronegative oxygen atom. Amongst three nitrogen atoms, the N30 atom has a more negative charge and the value of Mulliken atomic charge is  $-0.380112$ . The oxygen atom has  $-0.358140$  Mulliken atomic charge.

The MESP and contour plot for the **PIFHT** molecule is presented in Figures 9 and 10, respectively. The MESP plots for the rest of the molecules are depicted in Figure S3 (supporting information). The regions of positive, negative, and neutral potentials are indicated by different colors in the MESP plots. The red and yellow regions in the MESP plots relate to the region of high electron density and are associated with electrophilic reactivity. On the contrary, the blue parts represent low electron density and susceptible to nucleophilic reactivity. The MESP plots suggest that the benzene ring bonded to the thiazole ring is profoundly susceptible to aromatic electrophilic substitution reaction except for the **NIFHT-2** and **NIFHT-3** molecules. In all the 2-hydrazinyl thiazole derivatives, the blue part is situated at the NH group suggesting high reactivity towards basic reagents. The thicker area in contour diagram represents greater electrostatic field than the region with non-crowded contour lines. The red region in counter map represents higher electron density.

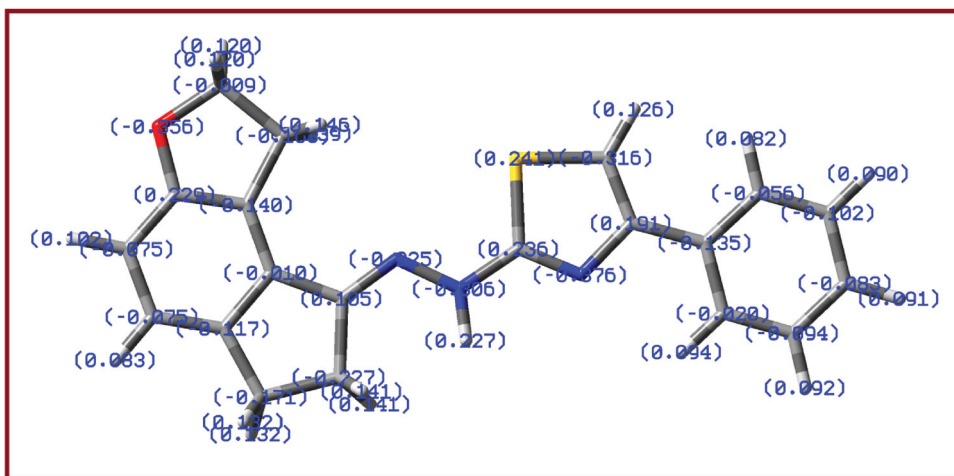


**Figure 8.** Mulliken atomic charge distribution in PIFHT molecule.

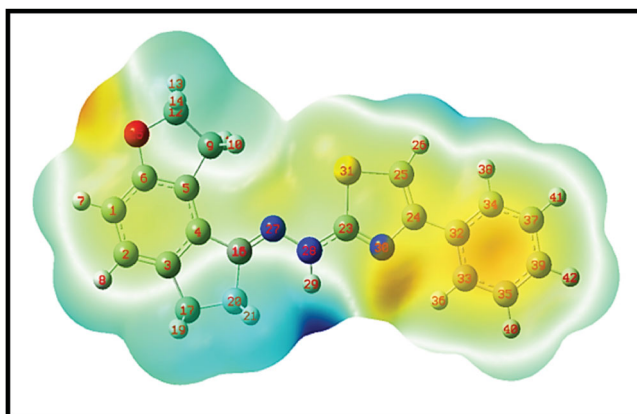


**Figure 9.** MESP plot of PIFHT molecule.

## 2.4. Vibrational assignments

The title molecule **PIFHT** has 42 atoms and therefore has 120 fundamental modes of vibration as per  $3N-6$  formula. The theoretical and experimental FT-IR spectra of **PIFHT** are depicted in Figures 11 and 12, respectively. Essentially all 120 fundamental modes of vibrations are IR active. The harmonic-vibrational frequencies were calculated for a **PIFHT** molecule at the B3LYP level using the 6-311G (d,p) basis set. The comparison between selected experimental and theoretical vibrational assignments is made and presented in Table S7 (supporting information). The theoretically computed IR spectrum often overestimates the vibrational bands; therefore a scaling factor of 0.96 was used to scale the computed frequencies [69]. The comparison has been made between the experimental frequencies and scaled vibrational frequencies. It has been found that there is good agreement between the scaled and experimental frequencies. The vibrational modes; symmetric and asymmetric stretching, deformation vibrations; in-plane bending and out of

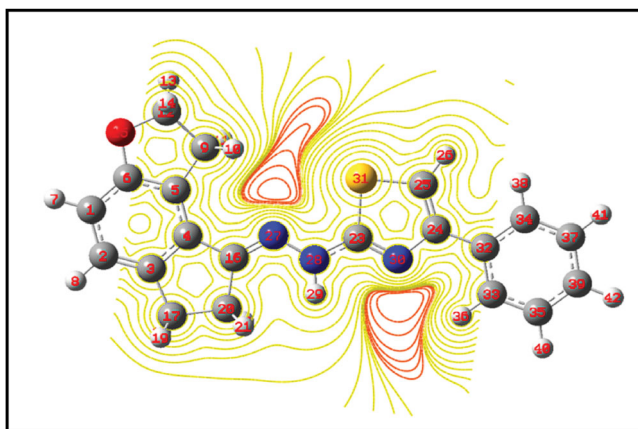


**Figure 10.** Contour surface of PIFHT molecule.

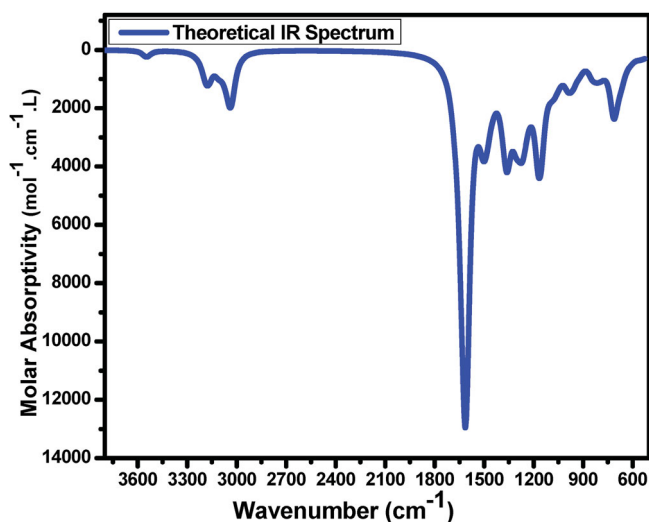


**Figure 11.** Theoretical IR spectrum of PIFHT.

plan bending, rocking, and twisting vibrations are present in the **PIFHT** molecule. The **PIFHT** contains imine groups, two benzene rings, and NH as main functional groups. Aromatic hydrocarbons have been found to show absorptions in the regions  $1600\text{--}1585\text{ cm}^{-1}$  and  $1500\text{--}1400\text{ cm}^{-1}$  due to the carbon-carbon stretching vibrations in the aromatic ring. Furthermore, they also show C-H stretching from  $3100\text{ to }3000\text{ cm}^{-1}$  and the in-plane bending occurs from  $1300\text{ to }1000\text{ cm}^{-1}$ . The experimental N31-H stretching vibration in the **PIFHT** molecule is at  $3405\text{ cm}^{-1}$ . The similar stretching vibration is at  $3415.93\text{ cm}^{-1}$  in the computed spectrum. The experimental and computed IR values of the N23 = C30 bond are  $1558$  and  $1560.41\text{ cm}^{-1}$ , respectively. The aromatic C = C bonds ranges from  $1560.41\text{ cm}^{-1}\text{--}1475.54\text{ cm}^{-1}$  in experimental IR and  $1493\text{ cm}^{-1}\text{--}1558\text{ cm}^{-1}$  in the computed IR spectrum. The experimental symmetric C9-H22 stretching vibration is  $2917\text{ cm}^{-1}$  while the theoretical IR value of the same bond is  $2914.44\text{ cm}^{-1}$ . Nearly all

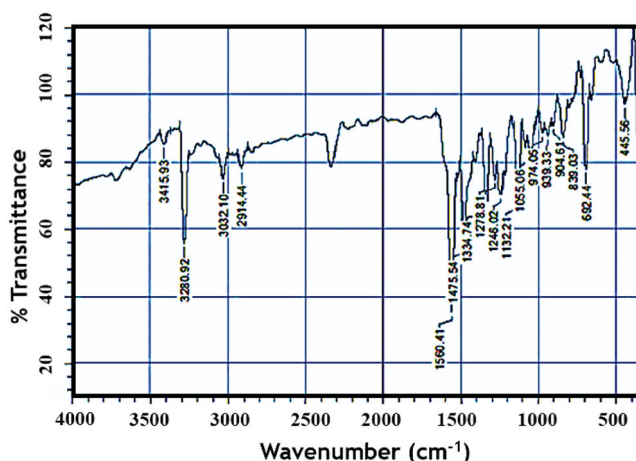


**Figure 12.** Experimental FT-IR spectrum of PIFHT.

important theoretical vibrational bands are having a good agreement with experimental results, and importantly, correct vibrational assignments have been made using computed vibrational frequencies.

### 3. Conclusion

In summary, we have explored various structural, chemical, electronic, and spectroscopic facets of ten 2-(2-hydrazineyl)thiazole derivatives by using the DFT method at B3LYP/6-311G (d,p) and TD-DFT at B3LYP/6-311G (d,p) level of theory. The structural exploration revealed that all molecules are non-planar with C1 point group symmetry; however, individual aromatic rings are planar. For a detailed structural and spectroscopic (UV-Visible and IR) analysis, the **PIFHT** as a representative molecule is discussed. The molecule **NIFHT-2** has the highest polarity whereas the molecule **IFHPT** has the lowest polarity amongst 2-(2-hydrazinyl)thiazoles. FMO analysis of all ten molecules was performed and the results indicate that the molecule **NIFHT-3** has the lowest energy gap amongst all molecules. This means that the inevitable charge transfer is easier in **NIFHT-3** as compared to other molecules. Various quantum chemical parameters have been computed to analyze the chemical nature of the molecules. Almost all important theoretical vibrational bands are having concurrence with experimental results, and importantly, correct vibrational assignments have been made using scaled vibrational frequencies. The MESP plots infer that the benzene ring attached to the thiazole ring is significantly prone to electrophilic attacks with the exception of the **NIFHT-2** and **NIFHT-3** molecules. The observed UV absorption bands can be assigned to  $\pi-\pi^*$  transitions and the correlation between the theoretical and experimental results is found to be satisfactory. The ICT phenomenon is dominant in the **NIFHT-2** and **NIFHT-3** molecules. The solvent dependence of the absorption band is observed to be less and can be attributed to the change in the transition dipole moments of the ground and excited states. The halogen substituents were found to diminish the UV absorption wavelength while other substituents ( $\text{NO}_2$ , OMe, Me, and Ar) augmented the same when compared with the phenyl ring.



## 4. Experimental

### 4.1. Experimental procedures and computational investigations

The 2-(2-hydrazineyl)thiazole derivatives were synthesized previously [40]. An FT-IR spectrum of the **PIFHT** compound was obtained on the SHIMADZU FT-IR spectrophotometer with potassium bromide pellets [40]. The experimental UV-Visible analysis was performed at 200–800 nm in DCM and DMSO solvents. DFT calculations were performed using the Gaussian-03 program package with Gauss View 4.1.2 molecular visualization program without any constraint on the geometry [70]. The geometry of the molecules is optimized by DFT/B3LYP method using a 6-311G (d,p) basis set. The FMO analysis and quantum chemical study were performed using the same basis set. Absorption energies ( $\lambda$  in nm), oscillator strength ( $f$ ), and transitions of all molecules have been calculated at TD-DFT B3LYP/6-311G (d,p) level of theory for B3LYP/6-311G (d,p) optimized geometries. The optimized structure of **PIFHT** was used in the vibrational frequency calculations at the same level of theory. To investigate the reactive sites of the title molecules, the molecular electrostatic surface potential plots were computed using the same method. Mulliken atomic charges were also explored using the same level of theory.

### Acknowledgments

Authors are grateful to Prof. (Dr.) A. B. Sawant for his generous help in the Gaussian study. The authors are also thankful to Mr. Sachin S. Shinde (Assistant professor), K.V.N Naik College, Nashik and RAP Analytical Research and Training Center, Nashik for UV-Visible spectral results. The CIC, KTHM College is acknowledged for FT-IR analysis. Authors acknowledge the Department of Chemistry, Arts, Science and Commerce College, Manmad, and Department of Chemistry, LVH Arts, Science and Commerce College Panchavati, Nashik for the laboratory facility.

### Disclosure statement

No potential conflict of interest was reported by the author(s).

### ORCID

Vishnu A. Adole  <http://orcid.org/0000-0001-7691-7884>

### References

- [1] Uchikawa O, Fukatsu K, Tokunoh R, et al. Synthesis of a novel series of tricyclic indan derivatives as melatonin receptor agonists. *J Med Chem.* 2002;45:4222–4239.
- [2] Kato K, Hirai K, Nishiyama K, et al. Neurochemical properties of ramelteon (TAK-375), a selective MT1/MT2 receptor agonist. *Neuropharmacology.* 2005;48:301–310.
- [3] Curreli F, Choudhury S, Pyatkin I, et al. Design, synthesis, and antiviral activity of entry inhibitors that target the CD4-binding site of HIV-1. *J Med Chem.* 2002;55:4764–4775.
- [4] Parrino B, Attanzio A, Spano V, et al. Synthesis, antitumor activity and CDK1 inhibition of new thiazole nortoposentin analogues. *Eur J Med Chem.* 2017;138:371–383.
- [5] Ayati A, Emami S, Asadipour A, et al. Recent applications of 1,3-thiazole core structure in the identification of new lead compounds and drug discovery. *Eur J Med Chem.* 2015;97:699–718.
- [6] Makam P, Kankanala R, Prakash A, et al. 2-(2-Hydrazinyl) thiazole derivatives: Design, synthesis and in vitro antimycobacterial studies. *Eur J Med Chem.* 2013;69:564–576.
- [7] Makam P, Thakur PK, Kannan T. In vitro and in silico antimalarial activity of 2-(2-hydrazinyl) thiazole derivatives. *Eur J Pharm Sci.* 2014;52:138–145.

- [8] Helal MHM, Salem MA, El-Gaby MS, et al. Synthesis and biological evaluation of some novel thiazole compounds as potential anti-inflammatory agents. *Eur J Med Chem.* **2013**;65:517–526.
- [9] Ignat A, Lovasz T, Vasilescu M, et al. Heterocycles 27. Microwave assisted synthesis and antitumour activity of novel phenothiazinyl-thiazolyl-hydrazine derivatives. *Arch Pharm.* **2012**;345:574–583.
- [10] Grozav A, Porumb ID, Găină LI, et al. Cytotoxicity and antioxidant potential of novel 2-(2-((1H-indol-5yl) methylene)-hydrazinyl)-thiazole derivatives. *Molecules.* **2017**;22:1–12.
- [11] Grozav A, Balacescu O, Balacescu L, et al. Synthesis, anticancer activity, and genome profiling of thiazolo arene ruthenium complexes. *J Med Chem.* **2015**;58:8475–8490.
- [12] Hassan AA, Ibrahim YR, El-Sheref EM. Synthesis and antibacterial activity of 4-aryl-2-(1-substituted ethylidene) thiazoles. *Arch Pharm.* **2013**;346:562–570.
- [13] Ouf SA, Gomha SM, Ewies MM, et al. Synthesis, characterization, and antifungal activity evaluation of some novel arylazothiazoles. *J Heterocycl Chem.* **2018**;55:258–264.
- [14] Piddock LJ. Understanding drug resistance will improve the treatment of bacterial infections. *Nat Rev Microbiol.* **2017**;15:639–640.
- [15] Bondock S, Fouda AM. Synthesis and evaluation of some new 5-(hetaryl) thiazoles as potential antimicrobial agents. *Synth Commun.* **2018**;48:561–573.
- [16] Tissaoui K, Raouafi N, Boujlel K. Electrogenerated base-promoted synthesis of N-benzylic rhodanine and carbamodithioate derivatives. *J Sulfur Chem.* **2010**;31:41–48.
- [17] Parrino B, Attanzio A, Spano V, et al. Synthesis, antitumor activity and CDK1 inhibition of new thiazole nortoposentin analogues. *Eur J Med Chem.* **2017**;138:371–383.
- [18] Gümüş M, Yakan M, Koca İ. Recent advances of thiazole hybrids in biological applications. *Future Med Chem.* **2019**;11:1979–1998.
- [19] Helal MHM, Salem MA, El-Gaby MSA, et al. Synthesis and biological evaluation of some novel thiazole compounds as potential anti-inflammatory agents. *Eur J Med Chem.* **2013**;65:517–526.
- [20] Jeankumar VU, Renuka J, Santosh P, et al. Thiazole-aminopiperidine hybrid analogues: Design and synthesis of novel Mycobacterium tuberculosis GyrB inhibitors. *Eur J Med Chem.* **2013**;70:143–153.
- [21] Abdel-Wahab BF, Abdel-Gawad H, Awad GE, et al. Synthesis, antimicrobial, antioxidant, anti-inflammatory, and analgesic activities of some new 3-(2'-thienyl) pyrazole-based heterocycles. *Med Chem Res.* **2012**;21:1418–1426.
- [22] Pember SO, Mejia GL, Price TJ, et al. Piperidinyl thiazole isoxazolines: a new series of highly potent, slowly reversible FAAH inhibitors with analgesic properties. *Bioorg Med Chem Lett.* **2016**;26:2965–2973.
- [23] Bastaki A. Diabetes mellitus and its treatment. *Int J Diabetes Metab.* **2005**;13:111–134.
- [24] Gao HD, Liu P, Yang Y, et al. Sulfonamide-1,3,5-triazine-thiazoles: discovery of a novel class of antidiabetic agents via inhibition of DPP-4. *RSC Adv.* **2016**;6:83438–83447.
- [25] Pandya DH, Sharma JA, Jalani HB, et al. Novel thiazole-thiophene conjugates as adenosine receptor antagonists: Synthesis, biological evaluation and docking studies. *Bioorg Med Chem Lett.* **2015**;25:1306–1309.
- [26] Shidore M, Machhi J, Shingala K, et al. Benzylpiperidine-linked diarylthiazoles as potential anti-Alzheimer's agents: synthesis and biological evaluation. *J Med Chem.* **2016**;59:5823–5846.
- [27] Watt K, Manzoni P, Cohen-Wolkowicz M, et al. Triazole use in the nursery: fluconazole, voriconazole, posaconazole, and ravuconazole. *Curr Drug Metab.* **2013**;14(2):193–202.
- [28] Ahmed SA, Kloezen W, Duncanson F, et al. *Madurella mycetomatis* is highly susceptible to ravuconazole. *PLoS Neglected Trop Dis.* **2014**;8:1–4.
- [29] El-Zahar MI, El-Karim S. Schistosomiasis (chemoprophylaxis and treatments). *Egypt Pharm J.* **2012**;11:1–15.
- [30] Whitfield KC, Bourassa MW, Adamolekun B, et al. Thiamine deficiency disorders: diagnosis, prevalence, and a roadmap for global control programs. *Ann N Y Acad Sci.* **2018**;1430:3–43.
- [31] Dhir S, Tarasenko M, Napoli E, et al. Neurological, psychiatric, and biochemical aspects of thiamine deficiency in children and adults. *Front Psychiatry.* **2019**;10:207–221.
- [32] Cabras P, Schirra M, Pirisi FM, et al. Factors affecting imazalil and thiabendazole uptake and persistence in citrus fruits following dip treatments. *J Agric Food Chem.* **1999**;47:3352–3354.

- [33] Turiel E, Martín-Esteban A. Molecularly imprinted stir bars for selective extraction of thiabendazole in citrus samples. *J Sep Sci*. 2012;35:2962–2969.
- [34] Ramsey C, MacGowan AP. A review of the pharmacokinetics and pharmacodynamics of aztreonam. *J Antimicrob Chemother*. 2016;71:2704–2712.
- [35] Crandon JL, Nicolau DP. Human simulated studies of aztreonam and aztreonam-avibactam to evaluate activity against challenging gram-negative organisms, including metallo- $\beta$ -lactamase producers. *Antimicrob Agents Chemother*. 2013;57:3299–3306.
- [36] Mikamo H, Yin XH, Hayasaki Y, et al. Penetration of ravuconazole, a new triazole antifungal, into rat tissues. *Chemotherapy*. 2002;48:7–9.
- [37] Teixeira de Macedo Silva S, Visbal G, Lima Prado Godinho J, et al. In vitro antileishmanial activity of ravuconazole, a triazole antifungal drug, as a potential treatment for leishmaniasis. *J Antimicrob Chemother*. 2018;73:2360–2373.
- [38] Scatena CD, Kumer JL, Arbitrario JP, et al. Voreloxin, a first-in-class anticancer quinolone derivative, acts synergistically with cytarabine in vitro and induces bone marrow aplasia in vivo. *Cancer Chemother Pharmacol*. 2010;66:881–888.
- [39] Walsby EJ, Coles SJ, Knapper S, et al. The topoisomerase II inhibitor voreloxin causes cell cycle arrest and apoptosis in myeloid leukemia cells and acts in synergy with cytarabine. *Haematologica*. 2011;96:393–399.
- [40] Adole VA, More RA, Jagdale BS, et al. Efficient synthesis, antibacterial, antifungal, antioxidant and cytotoxicity study of 2-(2-hydrazineyl) thiazole derivatives. *ChemistrySelect*. 2020;5:2778–2786.
- [41] Burke K. Perspective on density functional theory. *J Chem Phys*. 2012;136:1–10.
- [42] Sawant AB, Nirwan RS. Synthesis, characterization and DFT studies of 6,8-dichloro-2-(4-chlorophenyl)-4H-chromen-4-one. *Indian J Pure Appl Phys*. 2012;50:308–313.
- [43] Wu J. Density functional theory for chemical engineering: from capillarity to soft materials. *AIChE J*. 2006;52:1169–1193.
- [44] Bernardi F, Bottoni A, Garavelli M. Exploring Organic Chemistry with DFT: Radical, Organometallic, and Bio-organic Applications. *Quant Struct Relationships*. 2002;21:128–148.
- [45] Adole VA, Jagdale BS, Pawar TB, et al. Molecular structure, frontier molecular orbitals, MESP and UV-visible spectroscopy studies of Ethyl 4-(3, 4-dimethoxyphenyl)-6-methyl-2-oxo-1, 2, 3, 4-tetrahydropyrimidine-5-carboxylate: A theoretical and experimental appraisal. *Mat Sci Res India*. 2020;17:13–36.
- [46] Zhang M, Dou M, Yu Y. DFT study of CO<sub>2</sub> conversion on InZr<sub>3</sub> (110) surface. *Phys Chem Chem Phys*. 2017;19:28917–28927.
- [47] Tariq S, Khalid M, Raza AR, et al. Experimental and computational investigations of new indole derivatives: a combined spectroscopic, SC-XRD, DFT/TD-DFT and QTAIM analysis. *J Mol Struct*. 2020;1207:127803.
- [48] Chamundeswari SV, Samuel EJ, Sundaraganesan N. Molecular structure, vibrational spectra, NMR and UV spectral analysis of sulfamethoxazole. *SpectrochimActa A Mol Biomol Spectrosc*. 2014;118:1–10.
- [49] Pradeepa SJ, Boobalan MS, Tamilvendan D, et al. Spectra, electronic structure and molecular docking investigations on 3-(phenyl (p-tolylamino) methyl) naphthalen-2-ol—An experimental and computational approach. *J Mol Struct*. 2017;1135:53–66.
- [50] Khalid M, Ali A, Adeel M D, et al. Facile preparation, characterization, SC-XRD and DFT/DTDF study of diversely functionalized unsymmetrical Bis-Aryl- $\alpha$ ,  $\beta$ -unsaturated ketone derivatives. *J Mol Struct*. 2020;1206:127755.
- [51] Ibrahim MA, Halim SA, Roushdy N, et al. Synthesis, DFT study and photoelectrical characterizations of the novel 4-methoxyfuro [3,2:6,7]chromeno[2,3-e]benzo[b][1,4] diazepin-5(12H)-one. *Optik (Stuttg)*. 2018;166:294–306.
- [52] Vadagaonkar KS, Yang CJ, Zeng WH, et al. Triazolopyridine hybrids as bipolar host materials for green phosphorescent organic light-emitting diodes (OLEDs). *Dyes Pigm*. 2019;160:301–314.

- [53] Adole VA, Waghchaure RH, Pathade SS, et al. Solvent-free grindstone synthesis of four new (*E*)-7-(arylidene)-indanones and their structural, spectroscopic and quantum chemical study: a comprehensive theoretical and experimental exploration. *Mol Simul.* **2020**;46 :1045–1054.
- [54] Roushdy N, Farag AA, Ibrahim MA, et al. Synthesis, spectral characterization, DFT and photosensitivity studies of 1-[[[4-methoxy-5-oxo-5H-furo[3,2-g]chromen-6-yl] methylidene] amino]-4,6-dimethyl-2-oxo-1,2-dihydropyridine-3-carbonitrile(MFCMP). *Optik.* **2019**;178: 1163–1176.
- [55] Patil BN, Lade JJ, Vadagaonkar KS, et al. Pyrrolo [1, 2-a] quinoxaline-based bipolar host materials for efficient red phosphorescent OLEDs. *ChemistrySelect.* **2018**;3:10010–10018.
- [56] Hassan WM, Moustafa H, Hamed MN, et al. DFT calculations and electronic absorption spectra of some  $\alpha$ - and  $\gamma$ -Pyrone Derivatives. *SpectrochimActa A Mol Biomol Spectrosc.* **2014**;117:587–597.
- [57] Bagno A, Rastrelli F, Saielli G. Predicting  $^{13}\text{C}$  NMR spectra by DFT calculations. *J Phys Chem A.* **2003**;107:9964–9973.
- [58] Khan E, Khalid M, Gul Z, et al. Molecular structure of 1,4-bis (substituted-carbonyl) benzene: A combined experimental and theoretical approach. *J Mol Struct.* **2020**;1205:127633.
- [59] Raza AR, Nisar B, Khalid M, et al. A facile microwave assisted synthesis and structure elucidation of (3R)-3-alkyl-4, 1-benzoxazepine-2, 5-diones by crystallographic, spectroscopic and DFT studies. *SpectrochimActa A Mol Biomol Spectrosc.* **2020**;230:117995.
- [60] Tariq S, Raza AR, Khalid M, et al. Synthesis and structural analysis of novel indole derivatives by XRD, spectroscopic and DFT studies. *J Mol Struct.* **2020**;1203:127438.
- [61] Halim SA, Khalil AK. TD-DFT calculations, NBO analysis and electronic absorption spectra of some thiazolo [3, 2-a] pyridine derivatives. *J Mol Struct.* **2017**;1147:651–667.
- [62] Baroudi B, Argoub K, Hadji D, et al. Synthesis and DFT calculations of linear and nonlinear optical responses of novel 2-thioxo-3-N,(4-methylphenyl) thiazolidine-4 one. *J Sulfur Chem.* **2020**;41:310–325.
- [63] Boukabene M, Brahim H, Hadji D, et al. Theoretical study of geometric, optical, nonlinear optical, UV–Vis spectra and phosphorescence properties of iridium (III) complexes based on 5-nitro-2-(2', 4'-difluorophenyl) pyridyl. *Theor Chem Acc.* **2020**;139:1–11.
- [64] Hadji D, Brahim H. Structural, optical and nonlinear optical properties and TD-DFT analysis of heteroleptic bis-cyclometalated iridium (III) complex containing 2-phenylpyridine and picolinate ligands. *Theor Chem Acc.* **2018**;137:180–189.
- [65] Pathade SS, Adole VA, Jagdale BS, et al. Molecular structure, electronic, chemical and spectroscopic (UV-visible and IR) studies of 5-(4-chlorophenyl)-3-(3,4-dimethoxyphenyl)-1-phenyl-4,5-dihydro-1H-pyrazole: combined DFT and experimental exploration. *Mat Sci Res India.* **2020**;17:27–40.
- [66] Merouane A, Mostefai A, Hadji D, et al. Theoretical insights into the static chemical reactivity and NLO properties of some conjugated carbonyl compounds: case of 5-aminopenta-2, 4-dienal derivatives. *Monatsh Chem.* **2020**;151:1095–1109.
- [67] Halim SA, Ibrahim MA. Synthesis, DFT calculations, electronic structure, electronic absorption spectra, natural bond orbital (NBO) and nonlinear optical (NLO) analysis of the novel 5-methyl-8H-benzo[H]chromeno[2,3-b][1,6]naphthyridine-6(5H),8-dione (MBCND). *J Mol Struct.* **2017**;1130:543–558.
- [68] Koopmans T. Über die Zuordnung von Wellenfunktionen und Eigenwerten zu den einzelnen Elektronen eines atoms. *Physica.* **1934**;1(1–6):104–113.
- [69] Adole VA, Jagdale BS, Pawar TB, et al. Experimental and theoretical exploration on single crystal, structural, and quantum chemical parameters of (*E*)-7-(arylidene)-1,2,6,7-tetrahydro-8H-indeno[5,4-b] furan-8-one derivatives: A comparative study. *J Chin Chem Soc.* **2020**: 1–15. doi:10.1002/jccs.202000006.
- [70] Frisch MJ, Trucks GW, Schlegel HB, et al. Gaussian 03, Revision E.01. Wellingford (CT): Gaussian, Inc; **2004**.